In situ measurement of a newly created polar cap patch

D. A. Lorentzen,[1] J. Moen,[2,3] K. Oksavik,[1] F. Sigernes,[1] Y. Saito,[4] and M. G. Johnsen[5]

Received 21 May 2010; revised 17 August 2010; accepted 15 September 2010; published 21 December 2010.

[1] The Investigation of Cusp Irregularities 2 sounding rocket was launched 5 December 2008 at 1035 UT. We present an overview of the associated solar wind and auroral conditions, and we look in detail at the relationship between poleward moving auroral forms (PMAFs) and the creation of polar cap patches using ground-based optical and radar data as well as in situ data from the rocket payload. The solar wind was found to be dominated by a stable interplanetary magnetic field (IMF) $B_z < 0$ and by an IMF $B_y > 0$ situation. The aurora was characterized by a series of PMAFs throughout the period of interest. Associated with each PMAF were polar cap patches seen to emerge from the most poleward location of the PMAFs. On the basis of the available data, we present a conceptual model explaining the creation of the polar cap patches under the given solar wind and ionospheric conditions.

Citation: Lorentzen, D. A., J. Moen, K. Oksavik, F. Sigernes, Y. Saito, and M. G. Johnsen (2010), In situ measurement of a newly created polar cap patch, *J. Geophys. Res.*, *115*, A12323, doi:10.1029/2010JA015710.

1. Introduction

[2] Drifting polar cap patches are localized regions of enhanced *F* region plasma densities and enhanced 6300 Å (O I) emissions with scale sizes of several hundreds of kilometers [*Weber et al.*, 1984]. The high-density patches are seen to drift antisunward during interplanetary magnetic field (IMF) southward conditions from the cusp region and into the polar cap with velocities of several hundred meters per second, and they can have densities up to 10 times the ambient background [*Weber et al.*, 1986]. The patches are then seen to leave the polar cap and enter the nightside auroral oval [cf. *Lorentzen et al.*, 2004; *Moen et al.*, 2007]. These patches have been known to disrupt radio communication and navigation systems at polar latitudes due to the formation of plasma density irregularities [e.g., *Basu et al.*, 1990, 1998].

[3] Polar cap patches can be detected by both incoherent scatter radars [e.g., *Lockwood and Carlson*, 1992], and optical instrumentation [e.g., *Lorentzen et al.*, 2004]. The latter using, e.g., imagers or photometers, monitoring emission lines from oxygen, with the ^1D 6300 Å (O I) emission as the most prominent feature in the visible region. As O^+ ions with enhanced densities drift into the polar cap, these might charge exchange with the ambient O_2 molecules, creating O_2^+ ions. The newly created O_2^+ ions might in turn go through a charge capture process with *F* region electrons, creating excited oxygen atoms.

[4] Several reviews of polar cap patch formation and morphology have been made [e.g., *Tsunoda*, 1988; *Crowley*, 1996; *Basu and Valladares*, 1999; *Dandekar and Bullett*, 1999]. The patches are thought to originate at subauroral latitudes, where photo ionization from solar EUV radiation enhances the plasma densities [*Foster*, 1993]. The plasma is then thought to follow the large-scale ionospheric convection [*Foster et al.*, 2005], and end up in the cusp region where the enhanced plasma is structured into patches. The patches then follow the convection across the polar cap. Another proposed source of the enhanced plasma patches is soft particle precipitation in the cusp region [*Walker et al.*, 1999], causing significant ionization that can result in *F* region plasma drifting into the polar cap. One study has also shown how a patch can form in the polar cap due to particle precipitation inside a lobe cell [*Oksavik et al.*, 2006].

[5] However, most mechanisms for patch formation focus on dense solar-EUV plasma and are believed to operate at or near the dayside open-closed boundary (OCB), i.e., the region equatorward of the dayside 6300 Å cusp emissions. These mechanisms can be summarized in three groups [*Moen et al.*, 2006]:

[6] First is transient reconnection. Flux transfer events or transient reconnection is a possible structuring mechanism as presented by *Lockwood and Carlson* [1992], where the OCB leaps equatorward to a high-density plasma reservoir, followed by a relaxation of that boundary, carrying with it high-density plasma into the polar flow. *Carlson et al.* [2004, 2006] have successfully tested this mechanism.

[7] Second is plasma depletion. *Valladares et al.* [1996] suggest that the electron density depletion between patches is caused by an enhanced plasma recombination rate. This recombination is due to enhanced ion-frictional or Joule

[1]Geophysics Department, University Centre in Svalbard, Longyearbyen, Norway.
[2]Department of Physics, University of Oslo, Oslo, Norway.
[3]Geophysics Department, University Centre in Svalbard, Longyearbyen, Norway.
[4]Institute of Space and Astronautical Science, Japan Aerospace Exploration Agency, Sagamihara, Japan.
[5]Department of Physics and Technology, University of Tromsø, Tromsø, Norway.

0148-0227/10/2010JA015710

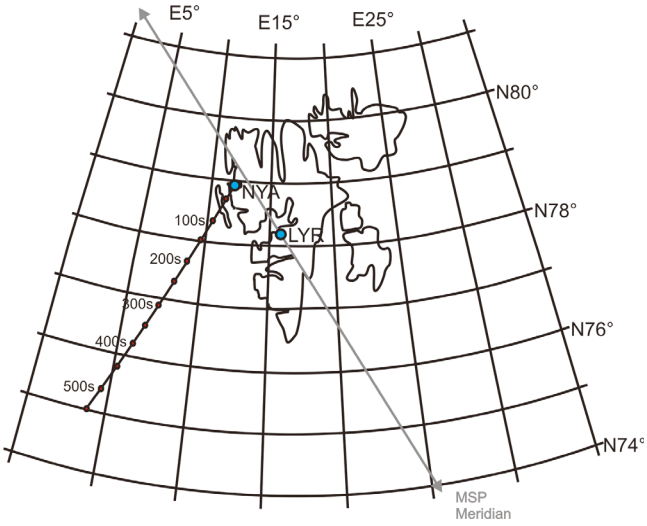

Figure 1. Overview map of Svalbard in geographic coordinates, showing the locations of the Ny-Ålesund (NYA) launch site and the Longyearbyen (LYR) observation site. Overlaying the map is the rocket trajectory, with flight time in seconds. The apogee point is at 302 s. Also included in the figure is the LYR MSP line of sight along the geomagnetic meridian plane.

heating from rapid plasma drift of short-lived east-west flow channels in the cusp region.

[8] Third is changing convection. *Anderson et al.* [1988] and *Sojka et al.* [1993, 1994] presented a mechanism which responds to changes in the convection pattern, especially in the IMF B_y component. It expands the polar cap to lower latitudes and brings higher-density plasma into the polar cap. The high-density plasma moves under the influence of the convection pattern from the solar-illuminated dayside throat region into the polar cap. To create isolated patches instead of a continuous tongue of ionization, the transport needs to be discontinuous and time dependent. The IMF regulation will cause alternating intake of high- and low-density plasma [*Anderson et al.*, 1988; *Rodger et al.*, 1994]. *Rodger et al.* [1994] suggest short-lived convection jets linked to flow channel events as another possible chopping mechanism, while *Schunk et al.* [1994] suggest traveling twin convection vortices.

[9] An auroral signature sometimes seen in the dayside ionosphere is poleward moving auroral forms (PMAFs) [*Fasel*, 1995; *Sandholt et al.*, 1990, 1998]. The PMAFs are attributed as an ionospheric signature of transient magnetopause reconnection, i.e., a flux transfer event where newly opened flux tubes are being convected poleward from the dayside oval over the polar cap. Recent studies have also associated PMAFs with flow shears; that is, the PMAFs occur between channels of reverse flow that are embedded in the antisunward convection [e.g., *Oksavik et al.*, 2004, 2005; *Rinne et al.*, 2007; *Moen et al.*, 2008].

[10] The Investigation of Cusp Irregularities 2 (ICI-2) sounding rocket was launched from Ny-Ålesund (NYA), Svalbard, Norway (78.9°N, 11.9°E, geographic coordinates; 76.4°N, 110.2°E CGM coordinates) at 1035 UT on 5 December 2008. In this paper, we will give an overview of the solar wind and auroral conditions during launch, and we will present ground-based and in situ data indicating a relationship between PMAFs and the creation of polar cap patches.

2. Instrumentation

[11] The instrumentation used in this study includes a meridian scanning photometer (MSP), an all-sky imager (ASI), the European Incoherent Scatter (EISCAT) Svalbard Radar (ESR), Super Dual Auroral Radar Network (SuperDARN), ACE satellite data, and in situ sounding rocket data of electron density and low-energy electron precipitation (10 eV–10 keV). Figure 1 shows an overview map of Svalbard in geographic coordinates. The NYA launch site and the Kjell Henriksen Observatory and ESR sites in Longyearbyen (LYR; 78.2°N, 16.0°E geographic coordinates; 75.4°N, 111.4°E CGM coordinates) is shown. Overlaid the map is the MSP field of view. Also included is the ICI-2 trajectory southwest of NYA.

[12] The *MSP* is a five-channel photometer with a mirror scanning from 0°N to 180°S along the local geomagnetic meridian plane. The emission wavelengths used in this study are 4278 Å (N_2^+ 1 NG), 5577 Å (O I) and 6300 Å (O I). The emission intensities measured in Rayleighs are absolutely calibrated using a NIST traceable calibration lamp.

[13] The ASI is an intensified all-sky camera with a 180° field of view fish-eye lens. It records emission intensities across the sky at several different wavelengths. For this study, the 6300 Å (O I) emission is used.

[14] The ESR consists of a 32 m steerable antenna and a 42 m static field-aligned antenna. Both observe electron density and temperature, ion temperature and ion velocity as a function of altitude. For this study, only data from the field-aligned antenna is used.

[15] SuperDARN is a collection of HF radars measuring the Doppler velocity of density irregularities in the ionosphere. The data from multiple radars can be used to produce ionospheric plasma convection maps [*Ruohoniemi and Baker*, 1998].

[16] The ACE satellite monitors the solar wind conditions, including the IMF and the solar wind density and velocity. For this study the satellite was located at about $X = 221$, $Y = 27$, $Z = 9.5$ R_E in GSM coordinates. With an average solar wind speed of about 400 km/s in the time period of interest, this indicates a lead time of about 59 min, i.e., the time it takes for any changes in the solar wind to manifest itself in the dayside polar ionosphere.

[17] The ICI-2 sounding rocket reached apogee in its nominal trajectory at 328.7 km altitude after 302 s flight time. The payload consisted of two different Langmuir probes for electron density measurements, a low-energy electron spectrometer (energy measurements between 10 eV and 10 keV), a solid-state spectrometer for electrons and ions (energy measurements >20 keV), and AC and DC electric field and wave experiments. In this study, we will use data from the low-energy spectrometer and the four-needle Langmuir probe [*Jacobsen et al.*, 2010; *Bekkeng et al.*, 2010].

3. Observations

[18] Figure 2 shows an overview of the morning hours of 5 December 2008, with data from the MSP and the ACE

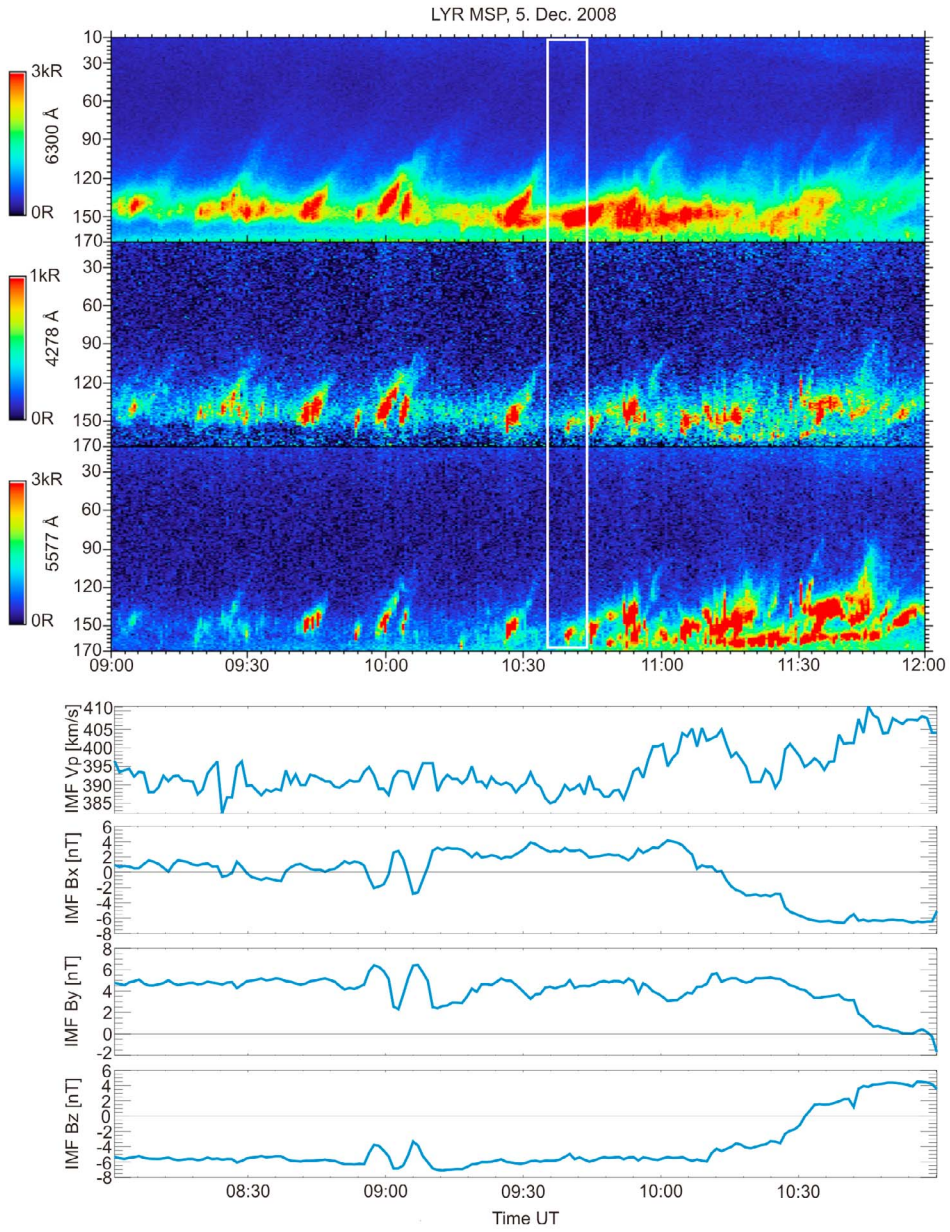

Figure 2. (top) Meridian scanning photometer (MSP) and ACE data, 5 December 2008, from 0900 to 1200 UT (MSP) and 0800 to 1100 UT (ACE; allowing for the calculated lead time of the ACE satellite of ~1 hour). From top to bottom, MSP 6300 Å emission intensities from 10°N to 170°S scan angle. Intensity is color coded in Rayleigh. The two next plots show the 4278 Å and 5577 Å emissions channels, respectively. The white box indicates the time of flight for the Investigation of Cusp Irregularities 2 (ICI-2) payload. (bottom) Data from ACE, including the solar wind speed in km/s and the IMF B_x, B_y, and B_z components in nT.

satellite. In Figure 2 (top), we see the 6300 Å, 4278 Å, and 5577 Å emissions, color coded in Rayleighs. Time is given in universal time on the x axis and scan angle from 10°N to 170°S along the meridian plane on the y axis. The white box indicates the time of rocket flight. In Figure 2 (bottom), we see the ACE radial speed in kilometers per second and the IMF B_x, B_y, and B_z components in nanoteslas. Universal time on the x axis has been shifted by ~1 hour compared to the MSP to account for the lead time of the ACE satellite.

[19] From the MSP we see that the dayside oval is located south of zenith, at about 140°–150° scan angle. We also see a number of auroral intensifications in the oval, apparent in all channels, followed by poleward expansions. These are characteristic MSP signatures of poleward moving auroral forms, especially distinctive in the 6300 Å emission channel. The PMAFs expand poleward to about 120°–90° scan angle, before the poleward boundary undergoes a rapid equatorward contraction. The repetition rate for the PMAFs seen in

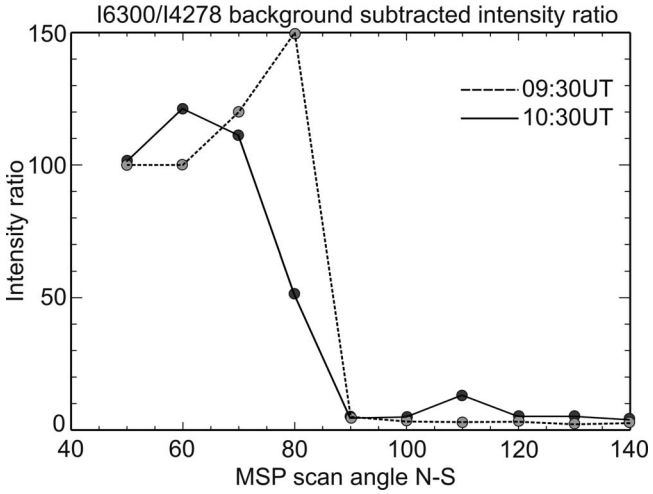

Figure 3. I6300/I4278 background subtracted intensity ratios. The dashed line follows the poleward moving auroral form (PMAF) later patch starting at about 0930 UT. The solid line follows the PMAF later patch starting at about 1030 UT.

Figure 2 varies from 15 to 27 min. We also note that the presence of >1 kR 4278 Å emissions with concurrent >3 kR 6300 Å emissions indicates a broad energy spectrum of the precipitating electrons. Postlaunch the 5577 Å emission intensity increases, while the 6300 Å emission intensity decreases. This indicates that the LYR (and NYA) station rotates out of the dayside cusp aurora and into the afternoon part of the auroral oval [*Sandholt et al.*, 1998].

[20] Another interesting feature seen in the MSP data is a series of intensifications seen to move into the polar cap, emerging from the most poleward location of the PMAFs. These very faint traces, seen in the 6300 Å channel from about 90°–60° scan angle, are MSP signatures of polar cap patches. To differentiate patch emissions from auroral emissions poleward of the dayside oval, a comparison between the 6300 Å channel and the 4278 Å channel (N_2^+) can be made, as patch emissions only are possible from excited oxygen atoms. From the 4278 Å channel, we clearly see that there is a lack of auroral emissions poleward of about 90° scan angle. In order to elucidate this point, Figure 3 shows two I6300/I4278 background-subtracted intensity ratio profiles. The dashed line follows the PMAF later patch starting at about 0930 UT for MSP scan angles from 140°S to 50°N. The solid line follows the PMAF later patch starting at about 1030 UT (close to launch time) for the same MSP scan angles. Equatorward of ~90° scan angle the intensity ratio has values from about 2 to 12, indicating auroral emissions. Poleward of ~90° scan angle the intensity ratio increases by more than an order of magnitude, implying the absence of 4278 Å N_2^+ emissions in this region, while still maintaining strong emission intensities for the 6300 Å wavelength. This indicates that the region poleward of ~90° scan angle is void of auroral precipitation, and that the characteristic 6300 Å emission signal seen in Figure 2 in this region, originates from a recombination process. (Note that if the emission signal equals the background signal, the result is put equal to one (not zero) in order to avoid infinity in the ratio.)

[21] Assuming patch altitudes in the *F* region, the meridional patch velocity can be easily calculated from the MSP data, yielding meridional velocities between 500 and 700 m/s for the patches observed between 0900 and 1100 UT.

[22] From the ACE data we see that the solar wind speed was about 390 km/s both prelaunch and during launch. We also note a slight increase in speed some 15 min after launch. The IMF is dominated by a steady negative IMF B_z of about −6 nT and a steady positive IMF B_y of about 4 to 5 nT. The IMF B_x component fluctuated around 0 nT, reaching a maximum of about 4 nT at the time of launch. This was also the general IMF configuration throughout the night and morning hours as well. The ACE particle detector experienced loss of signal during the time period of interest, but regained data acquisition at about 1100 UT, with measured solar wind densities of about 5 cm^{-3} (not shown).

[23] During the morning hours of 5 December 2008, the planetary *Kp* index was 1, increasing to 2 at about 0900 UT and reaching its maximum for that day with *Kp* = 4 at 1200 UT.

[24] Figure 4 shows ASI data at selected times (Figure 4, left), MSP 6300 Å channel (Figure 4, top right), and EISCAT 42 m field-aligned data (Figure 4, bottom right), in the time period 1000–1100 UT. The black stapled vertical line indicates the launch time of the ICI-2 sounding rocket.

[25] Starting with Figure 4 (top right), two distinct PMAFs were seen by the MSP at about 1002 and 1030 UT. In addition, we see faint traces of the newly created polar cap patches, starting in the south at about 90° scan angle moving northward into the polar cap. These patches can be visualized in the MSP data by taking profiles of intensity versus time for a given scan angle. The horizontal white line in the topmost plot indicates the location of the 98° scan angle profile shown in the plot below. We clearly see two double-humped peaks: one around 1010 UT and another around 1035 UT. The 98° scan angle of the MSP is coincident with the field of view of the 42 m ESR antenna.

[26] The next three plots on right hand side show ESR electron density and temperature and ion temperature. Combining the scan angle profile of the MSP with the ESR data, we see that when the radar is in the field of view of the PMAF/patch transition region, it records elevated electron densities ($>10^{11}$ m^{-3}) between 150 and 250 km altitude, with concurrent elevated electron temperatures, i.e., low-energetic particle precipitation in the *F* region. We also note no enhancement in the ion temperature during the two events (i.e., no local Joule heating over the ESR).

[27] The four leftmost plots, labeled 1–4 and designated hereafter as ASI-1 to ASI-4, show 6300 Å all-sky imager data from LYR. The images are overlaid a geographic reference frame with Svalbard in the center, as well as the geographic location of the MSP geomagnetic meridian plane (white line) and rocket path (solid dashed and, later, solid line). The corresponding universal times for the images are also marked on the MSP plot, using the same type of labels. ASI-1 (1022 UT) shows the situation for the most equatorward location of the oval in the time period of interest. We see that the oval is located well south of Svalbard, and from the MSP (as well as ASI images at other times; not shown) we see that this had been the persisting situation for more than 10 min. ASI-2 (1031 UT) shows the situation for the most poleward location of the poleward moving auroral

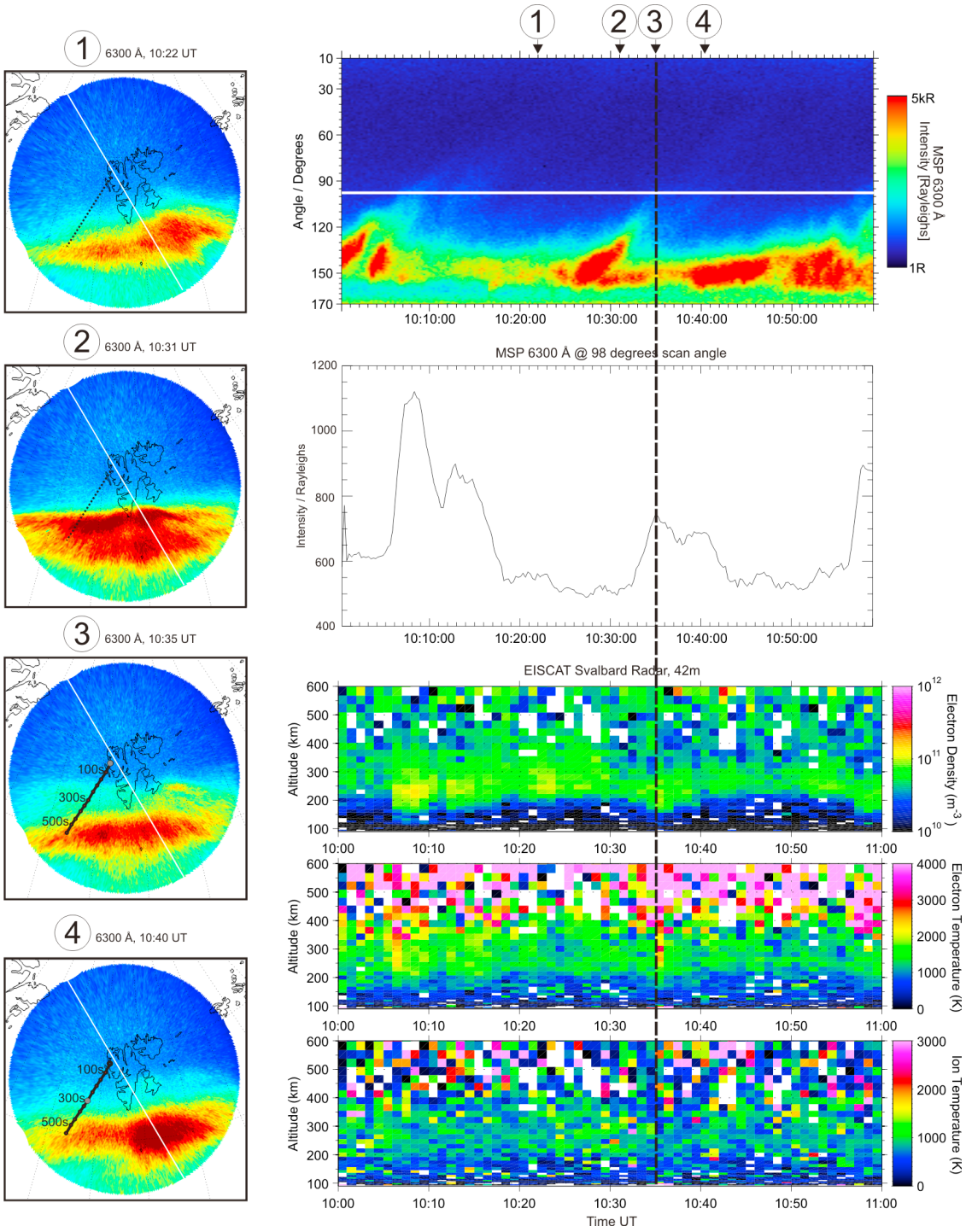

Figure 4. (right) MSP and European Incoherent Scatter Svalbard Radar (ESR) field-aligned data from 1000 to 1100 UT, 5 December 2008. (left) Also included are all-sky imager (ASI) data at selected times. The ASI data are mapped onto a geographical reference frame using a mapping altitude of 220 km. See the text for a detailed explanation.

form. We note a large increase in emission intensity, and that the poleward boundary of the 6300 Å emission is located close to the southern tip of Svalbard, or about 125° scan angle in the MSP. ASI-3 (1035 UT) shows the situation at launch time of the ICI-2 sounding rocket. The position of the rocket is marked as a shaded dot in this image. At the time of launch, the oval had retracted to a position similar to the situation seen in ASI-1. From ASI-3 we also see that in the wake of the retracting oval, there is a region of enhanced emission (compared to the background emissions) extending poleward to about LYR zenith. Comparing ASI-3 with ASI-2 (most poleward location of

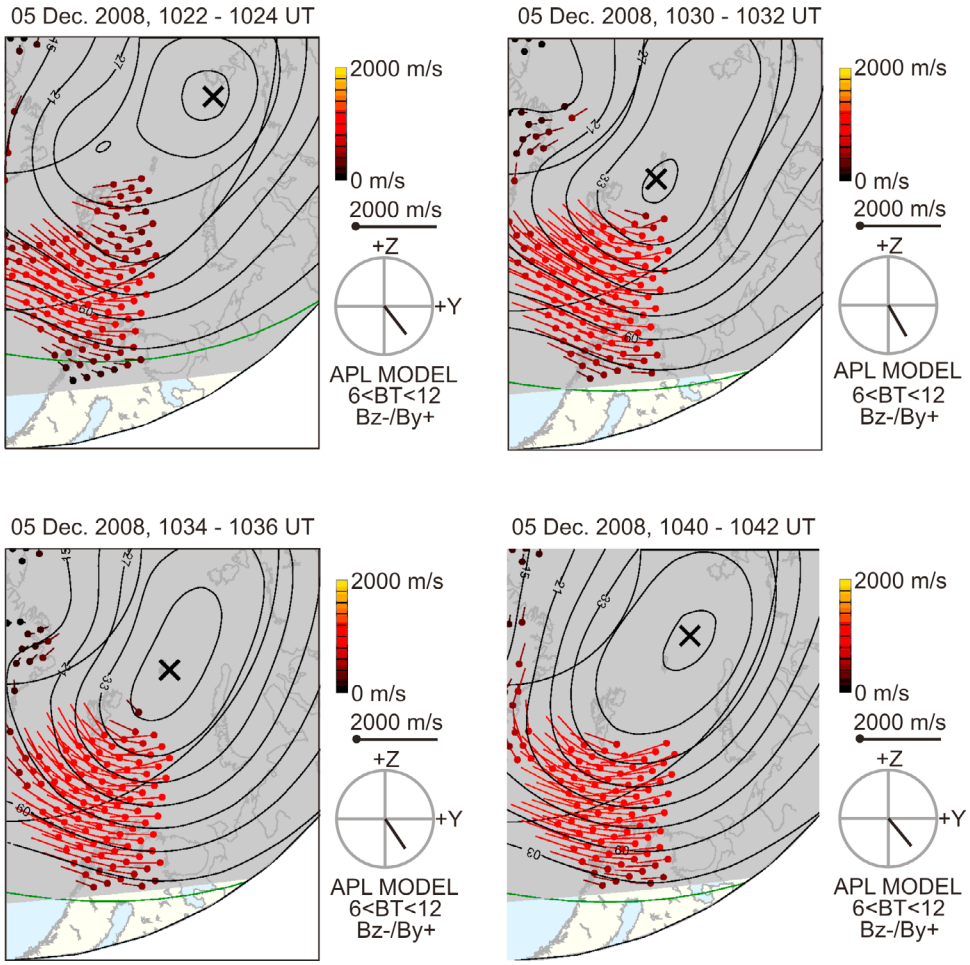

Figure 5. Super Dual Auroral Radar Network (SuperDARN) data at selected times, centered on Svalbard. The plots show flow vectors from the large-scale convection in the afternoon convection cell. Each plot covers approximately 20° in latitude.

PMAF) we also see that the enhanced emission has started to drift into the polar cap. It is in this context the ICI-2 rocket is launched. ASI-4 shows the auroral situation and position of the payload at apogee (302 s flight time; 1040:04 UT at an altitude of 328.7 km). At this instance in time, the extension of the oval is about the same as seen in ASI-3, but we note an intensity enhancement in the oval to the southeast of Svalbard. The payload is poleward of the oval proper, and traversing the region of enhanced emission.

[28] Figure 5 shows the large-scale convection pattern over Svalbard as seen by SuperDARN. The shaded area is poleward of the ground terminator. Svalbard is located postnoon MLT, and for the 1000–1100 UT time period, it has rotated into the afternoon convection cell. SuperDARN sees very strong backscatter south of Svalbard, with convection velocities greater than 1 km/s inside the dayside oval, moving in a northwesterly direction, consistent with the IMF B_y positive/IMF B_z negative situation. For the 1022–1024 UT period, coincident with the situation seen in ASI-1 (Figure 4) with no PMAF observed, we note that the convection velocities are generally lower, and that the backscatter is located further south than what is observed in the next three plots. From the 1030–1032 UT plot (corresponding to ASI-2 in Figure 4), the effect of the PMAF is seen in the radar data, with increased convection velocities and a poleward expansion of the main backscatter. This holds true also for the plots labeled 1034–1036 UT and 1040–1042 UT. Note that for the last three plots there are regions of enhanced velocities in the middle of the backscatter, with reduced velocities on the flanks.

[29] Data from the rocket payload is shown in Figure 6. The top plot shows data from the low-energy electron spectrometer from 200 s flight time (altitude ~283 km) to 500 s flight time (altitude ~155 km), passing through the apogee point at 302 s flight time (altitude ~329 km). As the payload is poleward of the oval proper, the measured electron energies are low (<150 eV) and with varying differential particle energy fluxes. We note two regions of inverted V-like signatures at ~310 s and ~400 s flight time. In the lower plot, data from the four-needle Langmuir probe (4-NLP) show electron density measurements, with the payload trajectory as a function of altitude overlaid. The maximum electron density (~1.2×10^{11} m^{-3}) is encountered early in the flight at about 130 s flight time and around 200 km altitude. Just

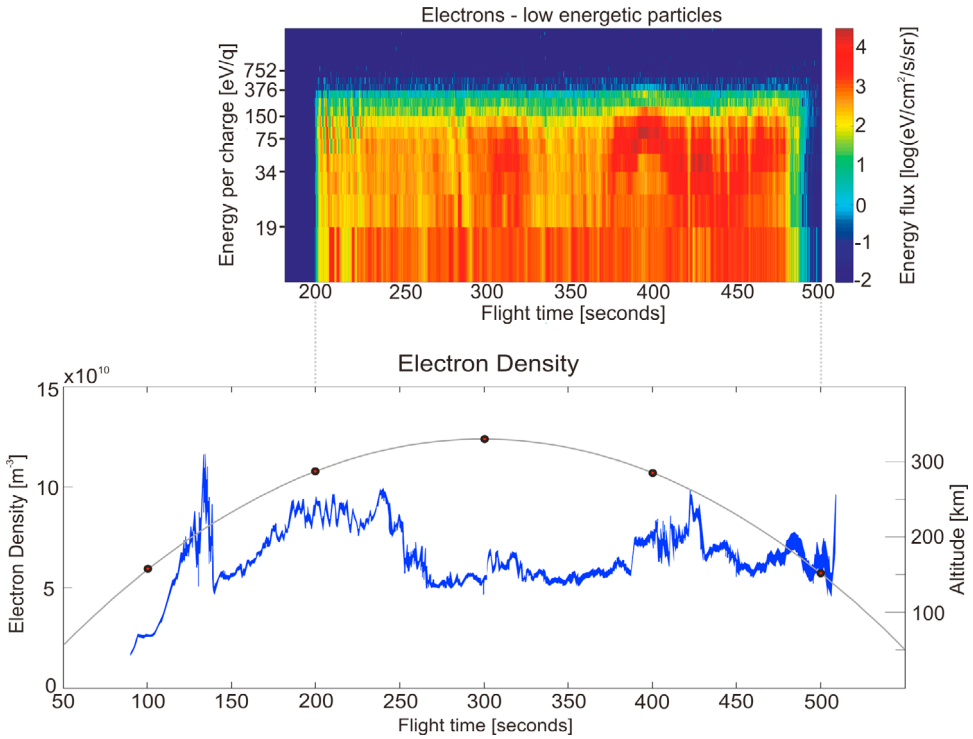

Figure 6. (top) ICI-2 low-energetic particles (LEP) and (bottom) four-needle Langmuir probe electron density data (4NLP). The LEP data are shown from 200 to 500 s flight time, with energy per charge as a function of seconds flight time, and with energy flux in eV/cm^2 s sr and color coded. The 4NLP data are shown from 50 to 550 s flight time, with electron density as a function of seconds flight time. Also shown in this plot is the payload altitude (right axis) as a function of seconds flight time.

after this, the density drops to about 5×10^{10} m^{-3}. Throughout the reminder of the flight, the electron density is seen to vary between 5 and 10×10^{10} m^{-3}.

4. Discussion

[30] The overall situation for the prelaunch hours can be characterized by a series of auroral forms moving westward and poleward (PMAFs; see Figures 2 and 4). For each PMAF, a polar cap patch is seen to emerge from the most poleward location of the PMAF, indicating an observational relationship between PMAFs and polar cap patches. The solar wind conditions are steady with negative IMF B_z and positive IMF B_y components of comparable magnitudes, and a solar wind speed of just below 400 km/s. This IMF configuration favors the development of PMAFs, but in general PMAF observations does not directly imply polar cap patch observations (compare *Sandholt and Farrugia* [2007], who presented PMAF data with IMF configuration, observational location and time of year matching this data set, but with no polar cap patch observations).

[31] The auroral 6300 Å emissions are "forbidden" transitions from atomic oxygen from the ^1D metastable state. The statistical residence time of the ^1D state is ~110 s, and the excited atom is thus susceptible to collisional quenching below ~200 km. This collisional deactivation of excited oxygen atoms in the ^1D state indicate that the main emission altitude of the 6300 Å emission line will be above 200 km. In addition, there is a vertical extent of the emission profile, which can extend more than 100 km [cf. *Solomon et al.*, 1988].

[32] At launch time, the solar elevation angles are approximately −11° for the LYR site and approximate −10° at rocket apogee (see Figure 1). This indicates that for the LYR and apogee positions, the atmosphere is sunlit above ~115 km and ~95 km, respectively.

[33] A model calculation of the portion of sunlit atmosphere as a function of universal time at the position of the payload apogee is shown in Figure 7. It is clearly seen that at *F*-layer altitudes (~300 km) the atmosphere is sunlit from ~0700 to ~1600 UT. For 200 km altitude, the corresponding times are ~0800 UT and ~1500 UT. Hence photoionization by direct sunlight is likely in the main emission region of the 6300 Å (O I) (i.e., above 200 km), throughout the period of interest.

[34] For the reminder of this paper we will concentrate on the time region around launch time. As stated in the observations section, a PMAF developed just prior to launch, and reached its most poleward location at 1031 UT (see ASI-2; Figure 4). We also stated that using the 6300 Å channel from the MSP, we observe polar cap patches emerging from the most poleward location of the PMAFs, and drifting into the polar cap. We will now argue that for this case study, PMAFs are the actuating mechanism needed for the creation of the observed polar cap patches.

[35] Figure 8 shows a 6 min period around launch time using the 6300 Å images of the ASI imager at LYR. Univeral time and seconds prelaunch and postlaunch are marked on each image. The images are ~30 s apart and

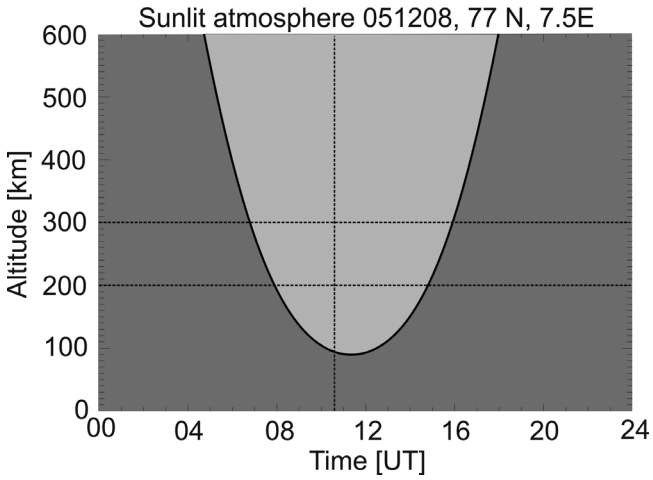

Figure 7. Model calculation of the portion of sunlit atmosphere (light shading) at latitude 77°N, and longitude 7.5°E (corresponding to payload apogee) as a function of altitude and UT time for 5 December 2008. The black vertical stapled line indicates the launch time of the ICI-2 sounding rocket. Black horizontal stapled lines are 200 and 300 km guidelines.

show the evolutionary stages of the polar cap patch, evident from the MSP in Figures 2 and 4 from about 1035 UT and onward. In Figure 8, solid lines (white or black) indicate unambiguous emission boundaries, while dashed lines (white or black) indicate ambiguous boundaries in the data. By the latter is meant emission boundaries that can only be inferred from a time series of data, i.e., extrapolated from near past or future data.

[36] The first image (1031:00 UT) shows the most poleward location of the PMAF. This image corresponds to ASI-2 in Figure 4. There is a clear emission boundary just south of LYR zenith (white solid line), and a more indistinct boundary further south between two local emission maxima (black dashed line). The latter situation is also confirmed in Figure 4, from the MSP data. The two local emission maxima are interpreted as a stable and continuous cusp emission (cusp proper) on the equatorward side, and separate flux tube(s) producing the distinct PMAF signature on the poleward side of the emission boundary. The boundary (black dashed line) is interpreted in terms of a flow channel event as introduced by *Southwood* [1987]. This flow channel would act as a separatrix between the cusp precipitation on the equatorward side, and the PMAF on the poleward side. According to *Southwood* [1985, 1987], there would be a weak return flow on either side of the boundary, indicated by weaker westward flows in these regions. Associated with the flux tube are Birkeland currents along the flanks of the tube to transfer stress from interplanetary space. *Oksavik et al.* [2004, 2005], and later *Rinne et al.* [2007] and *Moen et al.* [2008], have documented that there is indeed a close relationship between optical PMAF signatures and narrow flow channels. For the Northern Hemisphere and an IMF $B_y > 0$, $B_z < 0$ configuration at hand, the general large-scale convection will be westward in the cusp region, as indicated by the SuperDARN data (Figure 5). But *Oksavik et al.* [2005] has also documented that there is an even finer-scale current system and twin-cell flow pattern surrounding the PMAF, in agreement with the model of *Southwood* [1987]. As in the present case, the example of *Oksavik et al.* [2005] had a flow pattern that was too small to be fully resolved by SuperDARN, but the flow pattern was verified by DMSP satellite and EISCAT radar data. *Oksavik et al.* [2005, Figure 9] shows the geometry of the PMAF flow pattern and current system for the same IMF orientation. The PMAF will be in a region of upward current (i.e., electron precipication). Poleward of the PMAF the flow will have an eastward component, and equatorward of the PMAF the flow will be enhanced in the westward direction. Further equatorward there will be a region of downward current (i.e., void of aurora, similar to the minimum in the emissions along the dashed black line in Figure 8). The stable and continuous cusp aurora will be located further equatorward [*Oksavik et al.*, 2005]. Pedersen currents close the field-aligned current system in the ionosphere.

[37] Looking at the next few images in Figure 8, we see the situation associated with what would be termed a fast equatorward retraction of the PMAF if this was observed with the MSP, but using the ASI images we see a more detailed progression. Emission hot spots are developed poleward of the separatrix, indicated by white circles/ellipsoids, which as time progresses diminishes in intensity. This implies that the source region of the PMAF is turned off, while at the same time the cusp region (equatorward of the separatrix) is being maintained. Hence, as time progresses we end up with a region poleward of the separatrix consisting of enhanced emission, but with far lower intensity than the cusp proper. This indicates a region of enhanced plasma produced by both solar photoionization and local particle precipitation.

[38] The ICI-2 sounding rocket was launched into this region of enhanced plasma, and using Figures 6 and 8, we see that the payload hits the poleward boundary of the enhanced emission (white solid line, Figure 8) just prior to ASI 1037:00 UT (i.e., 118 s flight time). From the electron density plot in Figure 6, we see that the payload traverses the region of highest electron density experienced throughout the flight between 110 and 140 s flight time, corresponding to altitudes of 175 to 225 km, respectively, with electron densities greater than 1×10^{11} m^{-3}. From the last image in Figure 8, we see that a polar cap patch has been created on the westward side of Svalbard, a region governed by poleward convection as seen from the SuperDARN radar (Figure 5).

[39] The flow channel event indicates large field-aligned currents with associated Pedersen conductivity, the latter being enhanced by the solar-produced ionization. This indicates strong Joule heating which will produce an upwelling of the atmosphere, imposing a horizontal structure at *F* region altitudes.

[40] A polar cap patch can thereby be produced at *F* region altitudes from ambient solar produced ionization, together with locally vertically transported enhanced ionization from below *F* region altitudes. Figure 9 shows a cartoon of this model. At t_0 we have a situation corresponding to ASI-1 in Figure 4, i.e., cusp precipitation with no observed PMAF, but solar produced photo ionization at, and poleward of, the cusp region (shaded area). At t_1 a burst of transient

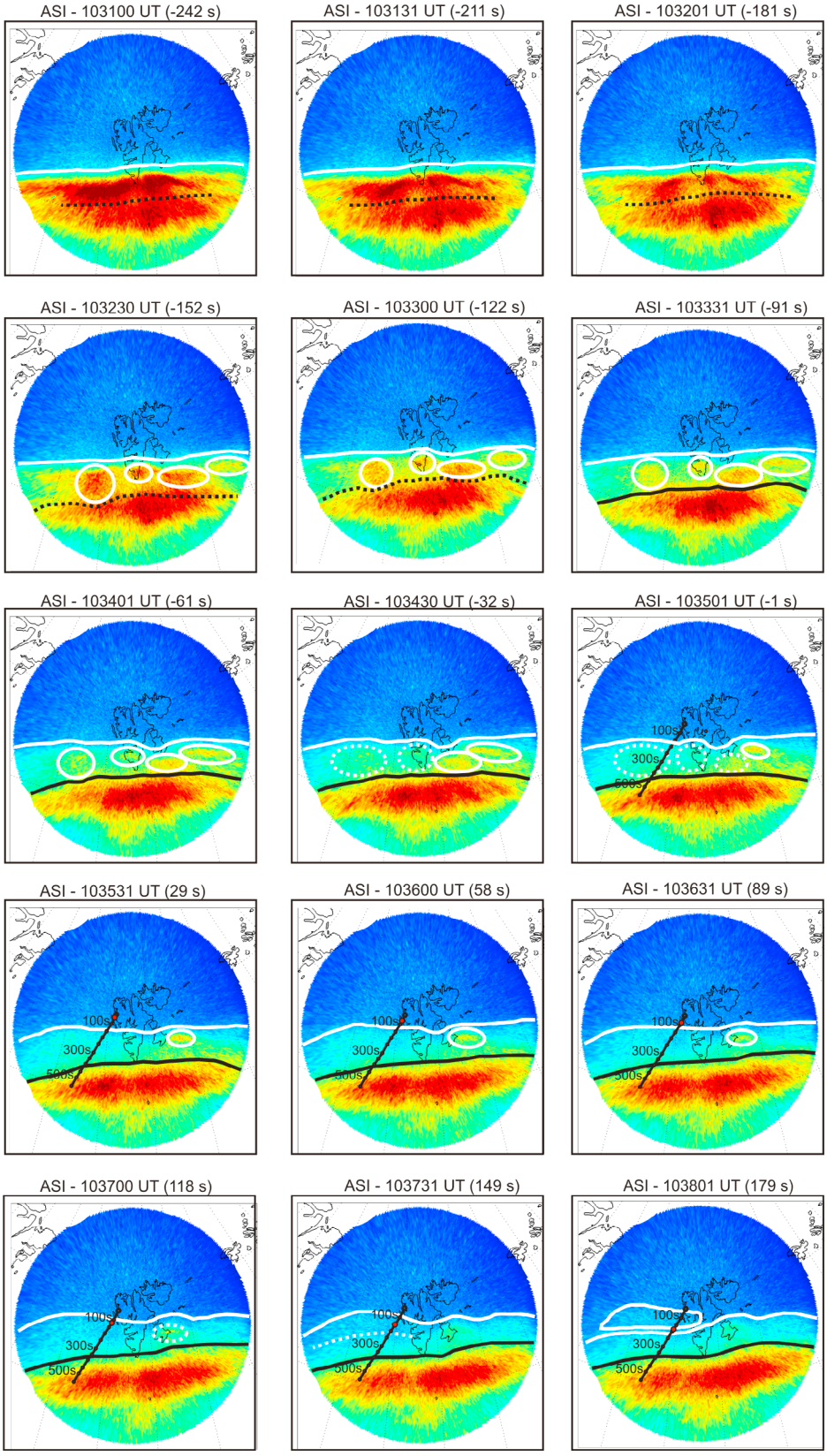

Figure 8. All-sky 6300 Å imager data for a 6 min period around launch time, showing the development of the associated cusp emissions, PMAF, and polar cap patch evolution. See the text for a detailed explanation.

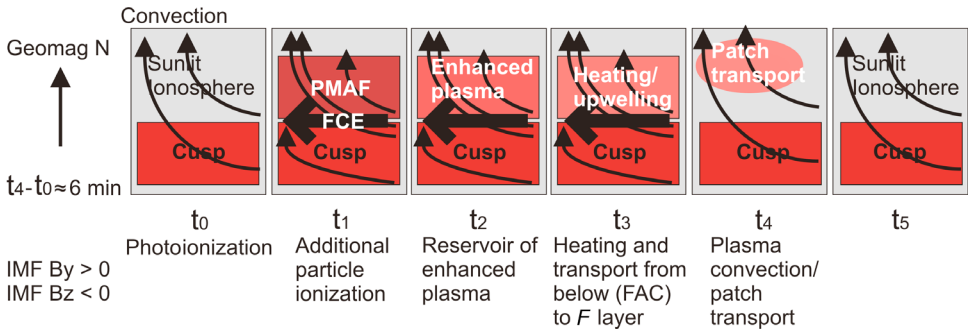

Figure 9. Cartoon of the proposed patch creation model. The cartoon is pertinent to the dayside Northern Hemisphere. See text for a detailed description.

reconnection occurs [*Lockwood and Carlson*, 1992] and the PMAF is observed poleward of the stable cusp precipitation. This introduces additional particle ionization above ~200 km [*Walker et al.*, 1999]. In addition, a flow channel event (FCE) is observed in the boundary between the cusp and PMAF emissions [*Southwood*, 1987; *Oksavik et al.*, 2004, 2005], acting as a separatrix between the two regions. This FCE will also lead to increased plasma depletion [*Valladares et al.*, 1996]. At t_2 the particle flux producing the PMAF is turned off, while still maintaining the cusp precipitation equatorward of the separatrix. This leaves a region of enhanced plasma poleward of the separatrix. At t_3 there is upward vertical transport of the enhanced plasma from below the *F* region, due to field-aligned currents and the enhanced Pedersen conductivity, resulting in strong localized Joule heating and corresponding upwelling of the atmosphere. Times t_2 and t_3 may be very close. At t_4 the density at *F* region altitudes is large enough to be differentiated from the background atmosphere by available measuring techniques (direct by radar, or indirect by optics), and the enhanced plasma can be observed moving poleward. At t_5 we are back to a similar situation as at t_0. This situation may then persist for ~10 min or more, until a new PMAF is observed and the patch creation process starts over again.

5. Conclusion

[41] We have presented a model of patch creation based on measurements obtained during the ICI-2 sounding rocket launch on 5 December 2008. Through a whole sequence of steps, this model unifies several ideas of traditional patch creation, e.g., transient reconnection plasma depletion, particle precipitation, and solar EUV produced plasma. In addition, it also involves additional steps like an upwelling lift of the patch to make it rise above the background plasma as a distinct feature.

[42] A series of PMAFs were observed ±2 hours around local geomagnetic noon (~0900 UT), and for each PMAF, patches of enhanced ionization were seen to move into the polar cap. The IMF conditions were steady throughout the period of interest with IMF $B_y > 0$ and IMF $B_z < 0$, and a solar wind speed of ~400 km/s. From our detailed study of the PMAF and patch observed around the time of liftoff of the ICI-2 rocket (1035 UT), we conclude the following:

[43] 1. The atmosphere above ~200 km had been sunlit for more than 2.5 hours prior to launch, indicating solar produced ionization above this altitude; that is, there exists a solar-produced tongue of ionization during the observation period.

[44] 2. There is an observational relationship between PMAFs and polar cap patches given the solar wind conditions referenced above; that is, when the precipitation faints and the 4278 Å emissions disappears, the poleward moving patches can be uniquely defined as a continuation of PMAFs.

[45] 3. From SuperDARN data, there is evidence of a FCE acting as a separatrix between a stable cusp precipitation and the PMAFs.

[46] 4. As the PMAF subsides, there is a region of enhanced density plasma (as evidenced by ICI-2 density data) and enhanced emission (as evidenced by all-sky imager data) poleward of the separatrix and equatorward of the lower density polar cap.

[47] 5. Associated with the FCE it is likely that there are strong Birkeland currents as well as enhanced Pedersen conductivity, acting to heat the atmosphere at these altitudes through Joule heating.

[48] 6. The heated atmosphere and field-aligned currents will result in an upwelling and transport of plasma from below up to *F* region altitudes.

[49] 7. When the density at *F* region altitudes is high enough, a polar cap patch can be observed moving poleward in the direction of the general convection.

[50] 8. In this data, there is no evidence for any equatorward leap of the OCB followed by a poleward relaxation in order to bring high-density plasma into the flow region.

[51] 9. In this data, there is no evidence for any apparent IMF B_y structuring concerning the creation of the polar cap patches.

[52] **Acknowledgments.** The Kjell Henriksen Observatory (KHO) is owned and operated by UNIS. EISCAT is an international association supported by Finland (SA), France (CNRS), Germany (MPG), Japan (NIPR), Norway (NFR), and Sweden (SRC). We thank the ACE science center for providing solar wind data from the ACE spacecraft. We also thank the SuperDARN PIs for the use of the SuperDARN radar data. This work has been financed in part by the Norwegian Research Council, AirForce Office of Scientific Research, Air Force Material Command, USAF, under grant FA8655-10-1-3003 and COST action ES0803.

[53] Robert Lysak thanks Jan Sojka and another reviewer for their assistance in evaluating this paper.

References

Anderson, D. N., J. Buchau, and R. A. Heelis (1988), Origin of density enhancements in the winter polar cap ionosphere, *Radio Sci.*, *23*, 513–519, doi:10.1029/RS023i004p00513.

Basu, S., and C. Valladares (1999), Global aspects of plasma structures, *J. Atmos. Sol. Terr. Phys.*, *61*, 127–139, doi:10.1016/S1364-6826(98)00122-9.

Basu, S., S. Basu, E. MacKenzie, W. R. Coley, J. R. Sharber, and W. R. Hoegy (1990), Plasma structuring by the gradient drift instability at high latitudes and comparison with velocity shear driven processes, *J. Geophys. Res.*, *95*, 7799–7818, doi:10.1029/JA095iA06p07799.

Basu, S., E. J. Weber, T. W. Bullett, M. J. Keskinen, E. MacKenzie, P. Doherty, R. Sheehan, H. Kuenzler, P. Ning, and J. Bongiolatti (1998), Characteristics of plasma structuring in the cusp/cleft region at Svalbard, *Radio Sci.*, *33*, 1885–1899, doi:10.1029/98RS01597.

Bekkeng, T. A., K. S. Jacobsen, J. K. Bekkeng, A. Pedersen, T. Lindem, J. I. Moen, and J.-P. Lebreton (2010), Design of a novel multi-needle Langmuir probe system, *Meas. Sci. Technol.*, *21*, 085903, doi:10.1088/0957-0233/21/8/085903.

Buchau, J., B. W. Reinisch, E. J. Weber, and J. G. Moore (1983), Structure and dynamics of the winter polar cap *F* region, *Radio Sci.*, *18*, 995–1010, doi:10.1029/RS018i006p00995.

Carlson, H. C., Jr., K. Oksavik, J. Moen, and T. Pedersen (2004), Ionospheric patch formation: Direct measurements of the origin of a polar cap patch, *Geophys. Res. Lett.*, *31*, L08806, doi:10.1029/2003GL018166.

Carlson, H. C., J. Moen, K. Oksavik, C. P. Nielsen, I. W. McCrea, T. R. Pedersen, and P. Gallop (2006), Direct observations of injection events of subauroral plasma into the polar cap, *Geophys. Res. Lett.*, *33*, L05103, doi:10.1029/2005GL025230.

Crowley, G. (1996), *Critical Review on Ionospheric Patches and Blobs*, *Rev. Radio Sci.*, vol. 1, Oxford Univ. Press, New York.

Dandekar, B. S., and T. W. Bullett (1999), Morphology of polar-cap patch activity, *Radio Sci.*, *34*, 1187–1205, doi:10.1029/1999RS900056.

Fasel, G. (1995), Dayside poleward moving auroral forms: A statistical study, *J. Geophys. Res.*, *100*, 11,891–11,905, doi:10.1029/95JA00854.

Foster, J. C. (1993), Storm time plasma transport at middle and high latitudes, *J. Geophys. Res.*, *98*, 1675–1689, doi:10.1029/92JA02032.

Foster, J. C., et al. (2005), Multiradar observations of the polar tongue of ionization, *J. Geophys. Res.*, *110*, A09S31, doi:10.1029/2004JA010928.

Jacobsen, K. S., A. Pedersen, J. I. Moen, and T. A. Bekkeng (2010), A new Langmuir probe concept for rapid sampling of space plasma electron density, *Meas. Sci. Technol.*, *21*, 085902, doi:10.1088/0957-0233/21/8/085902.

Lockwood, M., and H. C. Carlson Jr. (1992), Production of polar cap electron density patches by transient magnetopause reconnection, *Geophys. Res. Lett.*, *19*, 1731–1734, doi:10.1029/92GL01993.

Lorentzen, D. A., N. Shumilov, and J. Moen (2004), Drifting airglow patches in relation to tail reconnection, *Geophys. Res. Lett.*, *31*, L02806, doi:10.1029/2003GL017785.

Moen, J., H. C. Carlson, K. Oksavik, C. P. Nielsen, S. E. Pryse, H. R. Middleton, I. W. McCrea, and P. Gallop (2006), EISCAT observations of plasma patches at sub-auroral cusp latitudes, *Ann. Geophys.*, *24*, 2363–2374, doi:10.5194/angeo-24-2363-2006.

Moen, J., N. Gulbrandsen, D. A. Lorentzen, and H. C. Carlson (2007), On the MLT distribution of *F* region polar cap patches at night, *Geophys. Res. Lett.*, *34*, L14113, doi:10.1029/2007GL029632.

Moen, J., Y. Rinne, H. C. Carlson, K. Oksavik, R. Fujii, and H. Opgenoorth (2008), On the relationship between thin Birkeland current arcs and reversed flow channels in the winter cusp/cleft ionosphere, *J. Geophys. Res.*, *113*, A09220, doi:10.1029/2008JA013061.

Oksavik, K., J. Moen, and H. C. Carlson (2004), High-resolution observations of the small-scale flow pattern associated with a poleward moving auroral form in the cusp, *Geophys. Res. Lett.*, *31*, L11807, doi:10.1029/2004GL019838.

Oksavik, K., J. Moen, H. C. Carlson, R. A. Greenwald, S. E. Milan, M. Lester, W. F. Denig, and R. J. Barnes (2005), Multi-instrument mapping of the small-scale flow dynamics related to a cusp auroral transient, *Ann. Geophys.*, *23*, 2657–2670, doi:10.5194/angeo-23-2657-2005.

Oksavik, K., J. M. Ruohoniemi, R. A. Greenwald, J. B. H. Baker, J. Moen, H. C. Carlson, T. K. Yeoman, and M. Lester (2006), Observations of isolated polar cap patches by the European Incoherent Scatter (EISCAT) Svalbard and Super Dual Auroral Radar Network (SuperDARN) Finland radars, *J. Geophys. Res.*, *111*, A05310, doi:10.1029/2005JA011400.

Rinne, Y., J. Moen, K. Oksavik, and H. C. Carlson (2007), Reversed flow events in the winter cusp ionosphere observed by the European Incoherent Scatter (EISCAT) Svalbard radar, *J. Geophys. Res.*, *112*, A10313, doi:10.1029/2007JA012366.

Rodger, A. S., M. Pinnock, J. R. Dudeney, K. B. Baker, and R. A. Greenwald (1994), A new mechanism for polar patch formation, *J. Geophys. Res.*, *99*, 6425–6436, doi:10.1029/93JA01501.

Ruohoniemi, J. M., and K. B. Baker (1998), Large-scale imaging of high-latitude convection with Super Dual Auroral Radar Network HF radar observations, *J. Geophys. Res.*, *103*, 20,797–20,811, doi:10.1029/98JA01288.

Sandholt, P. E., and C. J. Farrugia (2007), Role of poleward moving auroral forms in the dawn-dusk auroral precipitation asymmetries induced by IMF B_y, *J. Geophys. Res.*, *112*, A04203, doi:10.1029/2006JA011952.

Sandholt, P. E., M. Lockwood, T. Oguti, S. W. H. Cowley, K. S. C. Freeman, B. Lybekk, A. Egeland, and D. M. Willis (1990), Midday auroral breakup events and related energy and momentum transfer from the magnetosheath, *J. Geophys. Res.*, *95*, 1039–1060, doi:10.1029/JA095iA02p01039.

Sandholt, P. E., C. J. Farrugia, J. Moen, Ø. Noraberg, B. Lybekk, T. Sten, and T. Hansen (1998), A classification of dayside auroral forms and activities as a function of interplanetary magnetic field orientation, *J. Geophys. Res.*, *103*, 23,325–23,345, doi:10.1029/98JA02156.

Sojka, J. J., M. D. Bowline, R. W. Schunk, D. T. Decker, C. E. Valladares, R. Sheehan, D. N. Anderson, and R. A. Heelis (1993), Modeling polar cap *F* region patches using time varying convection, *Geophys. Res. Lett.*, *20*, 1783–1786, doi:10.1029/93GL01347.

Sojka, J. J., M. D. Bowline, and R. W. Schunk (1994), Patches in the polar ionosphere: UT and seasonal dependence, *J. Geophys. Res.*, *99*, 14,959–14,970, doi:10.1029/93JA03327.

Solomon, S., P. B. Hays, and C. J. Abreu (1988), The auroral 6300 Å emission: Observations and modeling, *J. Geophys. Res.*, *93*, 9867–9882, doi:10.1029/JA093iA09p09867.

Southwood, D. J. (1985), Theoretical aspects of ionosphere-magnetosphere-solar wind coupling, *Adv. Space Res.*, *5*, 7–14, doi:10.1016/0273-1177(85)90110-3.

Southwood, D. J. (1987), The ionospheric signature of flux transfer events, *J. Geophys. Res.*, *92*, 3207–3213, doi:10.1029/JA092iA04p03207.

Tsunoda, R. T. (1988), High-latitude *F* region irregularities: A review and synthesis, *Rev. Geophys.*, *26*, 719–760, doi:10.1029/RG026i004p00719.

Valladares, C. E., D. T. Decker, R. Sheehan, and D. N. Anderson (1996), Modeling the formation of polar cap patches using large plasma flows, *Radio Sci.*, *31*, 573–593, doi:10.1029/96RS00481.

Walker, I. K., J. Moen, L. Kersley, and D. A. Lorentzen (1999), On the possible role of cusp/cleft precipitation in the formation of polar-cap patches, *Ann. Geophys.*, *17*, 1298–1305, doi:10.1007/s00585-999-1298-4.

Weber, E. J., J. Buchau, J. G. Moore, J. R. Sharber, R. C. Livingston, J. D. Winningham, and B. W. Reinisc (1984), *F* layer ionization patches in the polar cap, *J. Geophys. Res.*, *89*, 1683–1694, doi:10.1029/JA089iA03p01683.

Weber, E. J., J. A. Klobuchar, J. Buchau, H. C. Carlson Jr., R. C. Livingston, O. de la Beaujardiere, M. McCready, J. G. Moore, and G. J. Bishop (1986), Polar cap *F* patches: Structure and dynamics, *J. Geophys. Res.*, *91*, 12,121–12,129, doi:10.1029/JA091iA11p12121.

M. G. Johnsen, Department of Physics and Technology, University of Tromsø, N-9037 Tromsø, Norway.

D. A. Lorentzen, J. Moen, K. Oksavik, and F. Sigernes, Geophysics Department, University Centre in Svalbard, N-9171 Longyearbyen, Norway. (dag.lorentzen@unis.no)

Y. Saito, Institute of Space and Astronautical Science, Japan Aerospace Exploration Agency, 3-1-1 Yoshinodai, Sagamihara, Kanagawa 229-8510, Japan.